CFD Analysis of 500 kW Horizontal-Axis Wind Turbine Blades: Straight and Bent Cases

Sharanappa V. Sajjan[1], R. A. Savanur[2], Vidyadhar Y. Mudkavi[1]
[1]Computational and Theoretical Fluid Dynamics Division
National Aerospace Laboratories(CSIR), Bangalore 560 017, INDIA
[2]BLDEA'S College of Engg. and Tech., Bijapur 586 103, India
e-mail: svsajjan@ctfd.cmmacs.ernet.in, rasavanur@yahoo.co.in, vm@ctfd.cmmacs.ernet.in

Abstract

Three-dimensional CFD results are presented for the flow over a straight and a deformed horizontal-axis 500 kW wind turbine blade to study the effect of blade flexibility on the power of the wind turbine. The implicit Reynolds averaged Navier-Stokes solver (IMPRANS) based on finite volume nodal point spatial discretisation scheme with dual time stepping approach and Baldwin-Lomax turbulence model was used for the computations. Bent shape due to aeroelastic effect was computed using off-line coupling of structural model with panel method. Computations were carried out for several wind speeds. Results for designed wind speed of 12 meter per second for both straight and deformed blades are presented here. In general, power output increases due to deformation at most wind speeds except when the speed goes well beyond design wind speed when the power actually decreases.

Keywords: Unsteady flows, RANS solvers, Implicit schemes, Dual time stepping, Wind turbines

1 Introduction

Renewable energy from natural resources like wind, water and sun has found new emphasis in recent years due to the impending depletion of the non-renewable energy sources like coal and oil and ever increasing demand for energy due to rapid growth of the global industrialization. Consequently, the search for new and efficient methods to harness these available resources has prompted a fresh look at the existing technologies. A particular example of this renewed effort is provided by the wind turbines that have been in use at upper latitudes for some time now. Single machines of 2.5 to 3 Mega Watt capacity are currently in use. Design efforts for 5 MW capacity turbines are also being contemplated. On the other hand, it is difficult to extract large amount of energy in the tropics because of lower wind speeds that are prevalent in contrast to higher speeds in upper latitudes. Best speeds in the tropics tend to be nearly half of best speeds in the upper latitutes. While total wind potential in India is estimated to be about 65000 MW. In order to efficiently extract this energy, it is essential that turbines are designed for lower speeds appropriate for target sites. This is due to the fact that the power extracted varies as cube of wind speed and as such turbines designed for upper latitudes will operate sub-optimally in the tropics.

In a first of its kind, National Aerospace Laboratories, Bangalore, embarked on design of a 500 kW, low-cost, Horizontal-axis, two-bladed, downwind, teetered and stall regulated wind turbine. The design of an efficient wind turbine essentially depends on the design of the blades to provide the best aerodynamic characteristics to extract maximum energy from the wind. Considerable effort has been made to design efficient aerofoils having large lift to drag ratio and early stall characteristics [10, 13]. The diameter of this wind turbine turns out to be 45 meters. A similar sized turbine could extract much more energy in the upper latitudes. The blades are designed using composite materials and tend to be very slender and flexible. This flexibility of the turbine blade may have the effect on power output.

The complex nature of three-dimensional viscous unsteady flow field around a wind turbine blade proves to be a great challenge to the practitioners of computational fluid dynamics (CFD). Here, the rotating blade experiences a strong radial component of velocity. The flow field is normally characterized by strong tip vortices that are helical in shape. For multi-blade turbines, blade-vortex interaction can pose significant difficulties from fluid dynamics point of view. These problems arose first in the context of helicopter rotors. In that context, the need to evolve efficient methods for the design and performance analysis of rotors has led to the development of a number of techniques with increasing complexity. Of these, the simpler and faster methods are essentially based on the blade element momentum theory [8,9,11,14] and wake method [7, 8]. These methods now find applications for wind turbine as a natural extension.

The present work describes the three-dimensional viscous unsteady flow analysis of straight and the deformed blade to study the effect of blade flexibility on the power output using in-house developed code based on Reynolds averaged Navier-Stokes equations.

2 Computational Method

The RANS equations for three-dimensional unsteady compressible flow in a moving domain in nondimensional conservative form are given by

$$\frac{\partial \overline{U}}{\partial t} + \frac{\partial E}{\partial x} + \frac{\partial F}{\partial y} + \frac{\partial G}{\partial z} = 0. \tag{1}$$

Here, $\overline{U}$ is the vector of conserved variables, E,F and G are flux vectors, (x, y, z) is the Cartesian coordinate system and t is the time variable.

The governing equations (1) are solved by employing a dual time method with an implicit finite volume nodal point spatial discretisation [2, 3, 4, 5, 6]. Application of an implicit second order accurate backward difference formula for discretisation in real time and Euler's implicit time differencing formula for pseudo time leads to the following basic equation (2) of the implicit dual time stepping technique:

$$\left[I + \frac{3\Delta t^*}{2\Delta t} I + \Delta t^* \left(\frac{\partial R}{\partial U} \right)^m \right] \Delta U^m = -\Delta t^* \left[R(U^m) + \frac{3U^m}{2\Delta t} - \frac{2\overline{U}^n}{\Delta t} + \frac{\overline{U}^{n-1}}{2\Delta t} \right]. \tag{2}$$

Here $U^m = U(t^*) = U(m\Delta t^*)$ is the solution vector at pseudo time level m and $\Delta U^m = U^{m+1} - U^m$ is the change in U^m over the time step Δt^*, Δt denotes the real or physical time step that is required to resolve the physical unsteadiness of the flow. The barred quantities denote the solution vectors at the previous real time levels n and $n-1$ whereas R represents the spatial operators which give rise to the flux residual after a discretisation in space.

To facilitate the finite volume formulation, equations (2) are written in integral form and the surface integrals are evaluated by summing up the contributions due to the flux terms over the six faces of the computational cell. Applying integral conservative equations to each control volume, linearizing the changes in flux vectors using Taylor's series expansions in time, assuming locally constant transport properties, and dropping the superscript m we obtain

$$\begin{aligned}
&\left(I + \frac{3\Delta t^*}{2\Delta t} I \right) \Delta U_{ijk} + \frac{\Delta t^*}{\Omega_{ijk}} \sum_{m=1}^{6} \left\{ \left[\left(A - \frac{\partial E_R}{\partial x} \right) \Delta U \right]_m S_{mx} \right. \\
&\quad \left. + \left[\left(B - \frac{\partial F_S}{\partial y} \right) \Delta U \right]_m S_{my} + \left[\left(C - \frac{\partial G_T}{\partial z} \right) \Delta U \right]_m S_{mz} \right\} \\
&\quad = -\frac{\Delta t^*}{\Omega_{ijk}} \left\{ \sum_{m=1}^{6} \left[(E_I - E_V)_m S_{mx} + (F_I - F_V)_m S_{my} + (G_I - G_V)_m S_{mz} \right] \right\} \\
&\qquad\qquad -\Delta t^* \left(\frac{3U_{ijk}}{2\Delta t} - \frac{2\overline{U}^n_{ijk}}{\Delta t} + \frac{\overline{U}^{n-1}_{ijk}}{2\Delta t} \right),
\end{aligned} \tag{3}$$

Here Ω_{ijk} is the control volume surrounding the nodal point (i, j, k) of the curvilinear grid; $A = \partial E_I/\partial U$, $B = \partial F_I/\partial U$, $C = \partial G_I/\partial U$, $E_R = \partial E_{V_1}/\partial U_x$, $F_S = \partial F_{V_2}/\partial U_y$ and $G_T = \partial G_{V_3}/\partial U_z$ are the Jacobian matrices; E_I, F_I and G_I are the inviscid flux vectors and E_V, F_V and G_V are the viscous flux vectors; S_{mx}, S_{my} and S_{mz} are the x, y and z components of the surface vector corresponding to the m-th surface of the control volume.

The terms containing inviscid flux vectors can be calculated by using the flow variables at the six neighbouring points and Taylor's series expansions can be utilised to discretise the derivatives in the viscous flux terms directly in the physical plane. The resulting block tridiagonal system of equations are solved by using a suitable block tridiagonal solution algorithm and proper initial and boundary conditions. Turbulence closure is achieved through the algebraic eddy viscosity model of Baldwin and Lomax [1]. For a moving body, the equations are solved in the inertial frame of reference by employing a grid which remains fixed to the body and moves along with it. At each real time step $t + \Delta t$, starting from the solution at the previous time step t, the solution is marched in pseudo time t^* using local time stepping. Since the choice of physical time step Δt is no longer limited by stability considerations, a much larger time step, with a fixed but small number of inner iterations in pseudo time, can be used to reduce the undesirably large computational time for unsteady flow calculations. Based on this dual time stepping method an implicit Reynolds averaged Navier-Stokes solver IMPRANS has been developed at NAL for computing a wide range of three-dimensional unsteady viscous compressible flows. This RANS solver has been extensively validated for computing unsteady flow over aerofoils, wings, helicopter rotor blades and wind turbine blades [2, 3, 4, 5, 12].

2.1 Body motion

The governing equations (1) are written in the inertial frame of reference in which the body, along with the grid, translates and rotates in a prescribed manner. Suppose the body is first translated in such a manner that a point (x_c, y_c, z_c) fixed to the body moves to a new point (x'_c, y'_c, z'_c) and then rotated through angles (α, β, γ) about axes parallel to (x, y, z) axes respectively and passing through the centre of rotation (x'_c, y'_c, z'_c). The coordinates (x'_0, y'_0, z'_0) of an arbitrary point fixed to the body are given in terms of the coordinates (x_0, y_0, z_0) before the above translation and rotations as

$$\left\{ \begin{array}{c} x'_0 - x'_c \\ y'_0 - y'_c \\ z'_0 - z'_c \end{array} \right\} = [T] \left\{ \begin{array}{c} x_0 - x_c \\ y_0 - y_c \\ z_0 - z_c \end{array} \right\}, \tag{4}$$

where

$$[T] = [T_z][T_y][T_x], \tag{5}$$

$$[T_x] = \left[\begin{array}{ccc} 1 & 0 & 0 \\ 0 & \cos\alpha & -\sin\alpha \\ 0 & \sin\alpha & \cos\alpha \end{array} \right], \; [T_y] = \left[\begin{array}{ccc} \cos\beta & 0 & \sin\beta \\ 0 & 1 & 0 \\ -\sin\beta & 0 & \cos\beta \end{array} \right], \; [T_z] = \left[\begin{array}{ccc} \cos\gamma & -\sin\gamma & 0 \\ \sin\gamma & \cos\gamma & 0 \\ 0 & 0 & 1 \end{array} \right]. \tag{6}$$

When the translational velocities of the body along the (x, y, z) axes are given as $(\dot{x}_c, \dot{y}_c, \dot{z}_c)$ and the rotational velocities about the above axes passing through the point (x_c, y_c, z_c) are given as $(\dot{\alpha}, \dot{\beta}, \dot{\gamma})$, the velocities $(\dot{x}_0, \dot{y}_0, \dot{z}_0)$ of a point (x_0, y_0, z_0) fixed to the body are given by

$$\begin{aligned} (\dot{x}_0 - \dot{x}_c)\mathbf{e_x} \;+\; & (\dot{y}_0 - \dot{y}_c)\mathbf{e_y} + (\dot{z}_0 - \dot{z}_c)\mathbf{e_z} \\ = \; & (\dot{\alpha}\mathbf{e_x} + \dot{\beta}\mathbf{e_y} + \dot{\gamma}\mathbf{e_z}) \times [(x_0 - x_c)\mathbf{e_x} + (y_0 - y_c)\mathbf{e_y} + (z_0 - z_c)\mathbf{e_z}] \\ = \; & [\dot{\beta}(z_0 - z_c) - \dot{\gamma}(y_0 - y_c)]\mathbf{e_x} + [\dot{\gamma}(x_0 - x_c) - \dot{\alpha}(z_0 - z_c)]\mathbf{e_y} \\ & + [\dot{\alpha}(y_0 - y_c) - \dot{\beta}(x_0 - x_c)]\mathbf{e_z}, \end{aligned} \tag{7}$$

where $\mathbf{e_x}$, $\mathbf{e_y}$ and $\mathbf{e_z}$ are the unit vectors along the x, y and z axes respectively.

2.2 Initial and boundary conditions

The equations (1) are to be solved for given initial and boundary conditions. The initial conditions at $t = 0$, for impulsively started flow, are given as

$$u = \dot{x}_b, \quad v = \dot{y}_b, \quad w = \dot{z}_b, \quad \rho = 1, \quad e = \frac{1}{\gamma(\gamma-1)M_\infty^2} + \frac{1}{2}(\dot{x}_b^2 + \dot{y}_b^2 + \dot{z}_b^2), \tag{8}$$

at a point (x_b, y_b, z_b) on the solid boundary where the velocity components are $(\dot{x}_b, \dot{y}_b, \dot{z}_b)$ while, everywhere else,

$$u = U_0, \quad v = V_0, \quad w = W_0, \quad \rho = 1, \quad e = \frac{1}{\gamma(\gamma-1)M_\infty^2} + \frac{1}{2}(U_0^2 + V_0^2 + W_0^2), \tag{9}$$

where (U_0, V_0, W_0) are the free stream velocity components in the far field.
It may be noted that, for unsteady flow over a nonstationary body, the initial conditions can be chosen as any physically realizable state, for example, the steady flow obtained by assuming the body to be stationary at the condition at the initial instant.

Imposition of the no-slip condition for velocity and adiabatic wall condition for temperature at any time t leads to

$$\frac{\partial \rho}{\partial n} = \frac{\partial p}{\partial n} = 0, \quad u = \dot{x}_b, \quad v = \dot{y}_b, \quad w = \dot{z}_b, \tag{10}$$

at a point (x_b, y_b, z_b) on the solid boundary where n is the normal distance from the wall.
At the outer boundary, viscous effects are neglected and non-reflecting far field boundary conditions are constructed using the Riemann invariants for locally one-dimensional flow normal to the boundary [4].

3 Results and Discussion

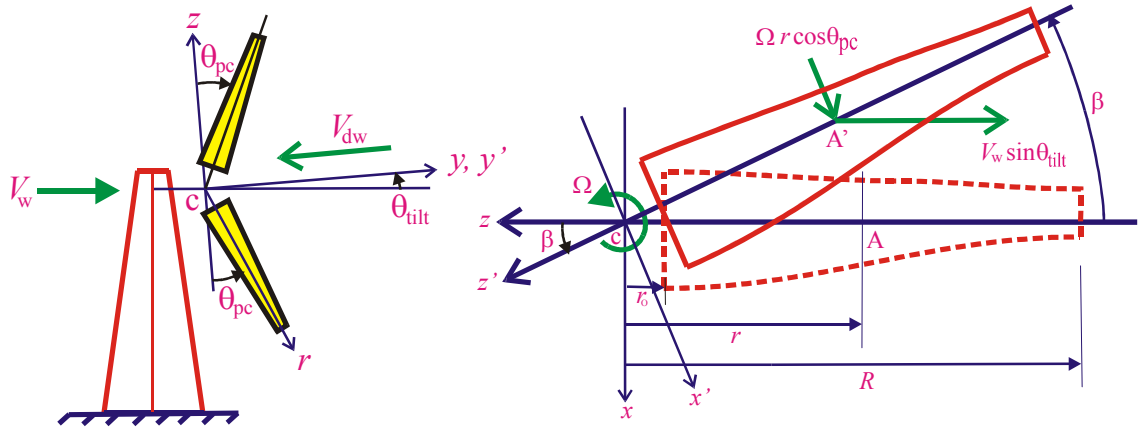

Figure 1: Schematic diagram of a wind turbine in yz and zx planes.

Owing to flexibility, the wind turbine blades undergo flexure due to aeroelastic effects. The bent shapes were determined by off-line coupling of ANSYS structrual model with in-house developed Panel method for airloads. The bent converged blade shapes for various wind speeds were obtained after three to four iterations. Following this, IMPRANS was used to simulate the flow field around a straight and a deformed wind turbine blade designed for an output of 500 kW at rated wind speed of 12 meter per second with a view to make an assessment of effect of flexure. This solver has been extensively validated for flow around the wind turbine blades for different wind velocities [2]. Figure 1, shows the schematic diagram of a two-bladed horizontal-axis downwind wind turbine in the yz plane (side view) and the plane of ratation zx or $z'x'$. Each turbine blade has a radius R with a precone of $\theta_{\rm pc}$ and the wind turbine axis is tilted by

an angle θ_{tilt} from the horizontal plane. The oncoming horizontal wind velocity is denoted by V_{w}, while the downwash velocity in the negative y or y' direction is given by V_{dw}. Here, (x, y, z) and (x', y', z') are the right-handed coordinate systems in the inertial and rotating frames of reference respectively and the rotation angles of the blade about the x', y' and z' axes are denoted by α, β and γ respectively. It may be noted here that the axes x', y' and z' are in chordwise, axial and radial directions with the origin of the coordinate system lying at the centre of rotation c(x_c, y_c, z_c). The blade rotates about the y or y' axis with an angular velocity Ω and the azimuthal angle β of the blade is set to zero at time t =0 when the blade axis lies on the negative z axis.

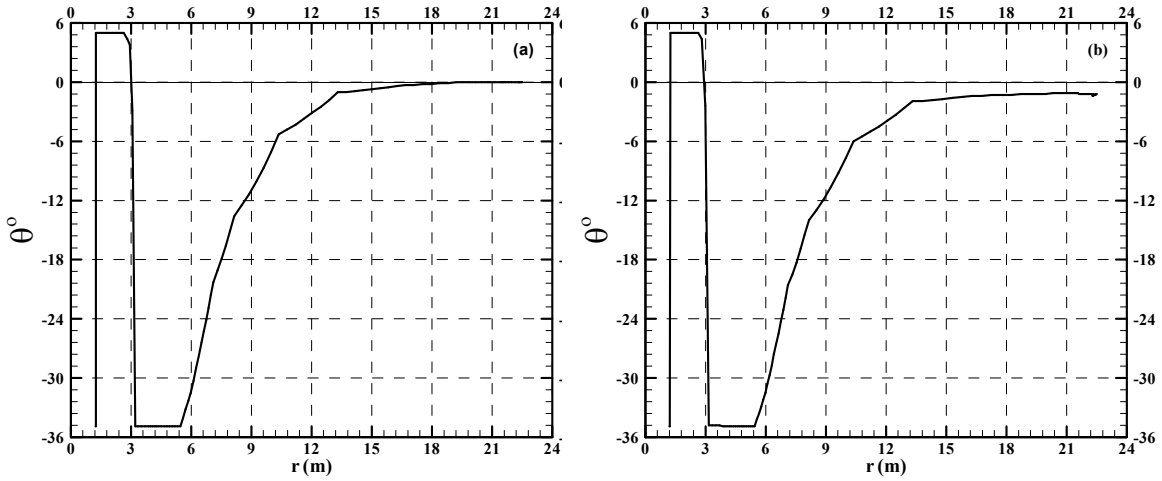

Figure 2: Distributions of twist θ on the 500 kW wind turbine straight (a) and deformed (b) blade of radius $R =$ 22.50 m.

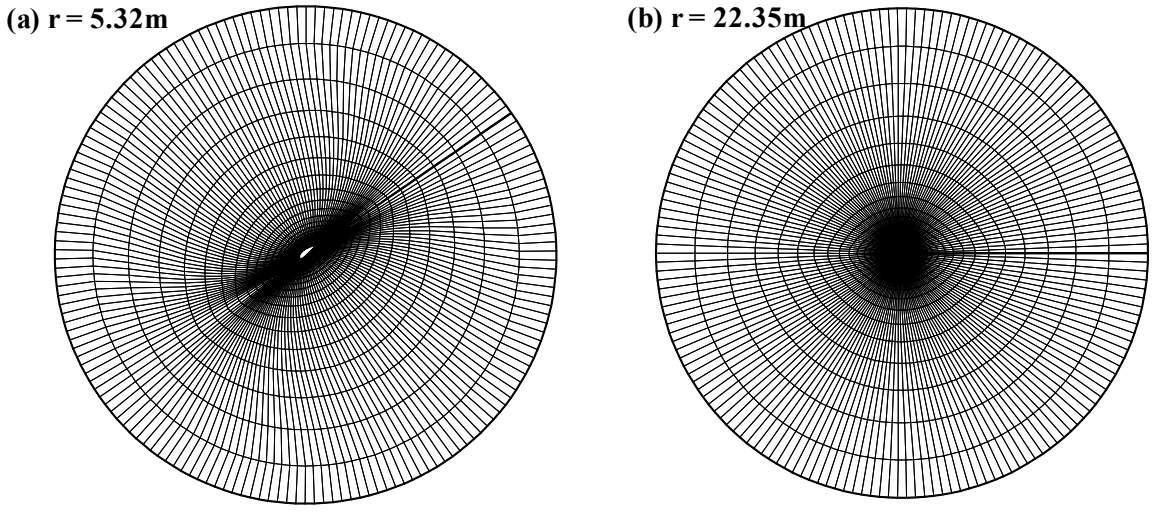

Figure 3: O-grids around two sections on a 500 kW wind turbine blade (straight) of radius R =22.5m.

The straight blade has a radius R = 22.5m and its root section, which is circular is offset by 1.24m. The chord of the blade sections decreases from 2.72m to 0.178m. The transition region, where the blade

section changes from a circular shape to an aerofoil shape, extends from r=0.178m to 1.25m. In figure 2, the distribution of twist θ for both straight blade (left) and deformed blade (right) are shown. As mentioned, the deformed blade configuration is obtained by coupling structural code with a panel method. For the stright blade configuration, the twist θ varies from -34.8° at section $r = 5.19$ m to zero at the tip, whereas for the deformed blade the twist θ varies from -34.8° at section $r = 5.19$ m to -2° at the tip.

A body conforming O-H type of grid is generated around the blade by using the commercial software GRIDGEN in such a way that grids are clustered properly near the leading and trailing edges and the tip, where the flow is expected to undergo rapid changes. The grid is nearly orthogonal at the surface, with the first grid point lying at 0.0005 m from the blade surface and 171, 71 and 127 grid points are chosen in the periodic, normal and spanwise (radial) directions respectively. There are 98 spanwise points on the blade and, 8 and 22 points lie beyond the root and tip. The outer grid boundary lies between two planes parallel to $x'y'$ plane lying at $z' = 1.3$ m and -21 m and a cylindrical surface of diameter of about 30 m with the blade lying on its axis. Typical sectional grids at $r = 5.32$ m and 22.35 m are shown in Figure 3.

Computation is carried out for both straight and deformed blades at a wind speed $V_{\rm w}$ of 12 m/s for which the turbine has been designed. The wind turbine here is provided with a tilt angle $\theta_{\rm tilt} = 7^\circ$ and precone $\theta_{\rm pc} = 6^\circ$. With the rotor RPM as 27 and the atmospheric conditions are taken as

$$T_\infty = 27^\circ{\rm C}, \quad c_\infty = 347.32{\rm m/s}, \quad \rho_\infty = 1.14{\rm kg/m}^3, \quad \nu_\infty = \mu_\infty/\rho_\infty = 16.05 \times 10^{-6}{\rm m}^2/{\rm s},$$

the tip Mach number $M_{\rm tip}$ and tip Reynolds number $Re_{\rm tip}$ are found to be 0.183 and 3.96 million and the tip speed ratio $\Omega R/V_{\rm w}$ for the above wind speed turns out to be 5.3. It may be noted that all the nondimensionalizing quantities, referred above with subscript ∞ refer to far field or free stream conditions except the length L_∞ and velocity U_∞ which are taken to be unity and tip velocity ΩR. The tip Reynolds number $Re_{\rm tip}$ here is defined by $\Omega R/\nu_\infty$. All variables are assumed to have been nondimensionalized. All the computations are carried out with the physical time step $\Delta t = 0.0392699082$ (which roughly corresponds to 0.1° rotation of the blade per time step) and with dual time stepping using 10 pseudo time steps. The specific heats ratio and the Prandtl number are taken to be 1.4 and 1 respectively. The second and the fourth order dissipation coefficients are chosen as 0 and 0.01 and transition point is fixed at the leading edge. All the computations are continued for 14400 time steps till the blade completes four full rotations when the flow is found to have almost reached the quasi-steady state. The aerodynamic

Wind Turbine	Power in kW using IMPRANS 3D	Thrust in kN using IMPRANS 3D	Power in kW using Panel Method	Thrust in kN using Panel Method
Straight blade	670.54	84.96	787.78	82.83
Deformed blade	723.20	86.60	824.01	87.70

Table 1: Aerodynamic Power and Thrust for Straight and deformed 500kW wind turbine blades.

power and thrust for both straight and deformed blade is given in table 1, for a rated wind speed of 12 meters per second by using IMPRANS and Panel codes. Results indicate that the power and thrust increases with the deformation of the blade. The surface pressure fields on the upper and lower surfaces of the straight turbine blade are shown in figure 4 and for the deformed blade in figure 5. Lower surfaces have always higher pressure which gives rise to thrust and subsequently power. Comparing the upper surfaces of the straight and deformed blades, it can be seen that deformed blade has slightly larger low-pressure area, which could be the reason for deformed blade has predicted more power. In figure 6, the

sectional pressure fields at different radial stations of both straight (left) and deformed (right) turbine blades are shown. Streamtraces for straight (left) and deformed (right) turbine blades at different radial sections are plotted in Figure 8.

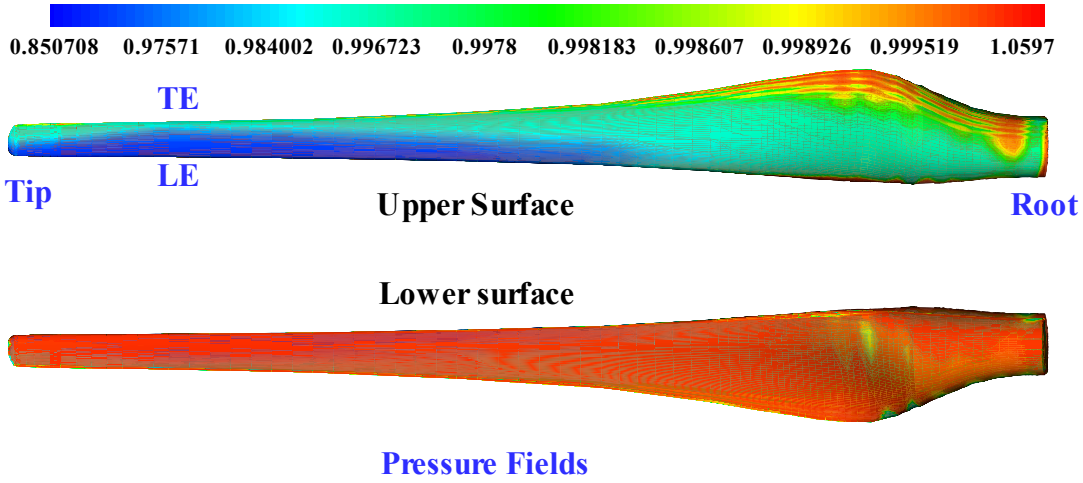

Figure 4. Pressure fields on the upper and lower surfaces of NAL's 500 kW wind turbine blade (straight). Tilt = 7^o; Precone = 6^o; Tip speed ratio = 5.3; $M = 0.183$; $Re = 3.96$ million per meter.

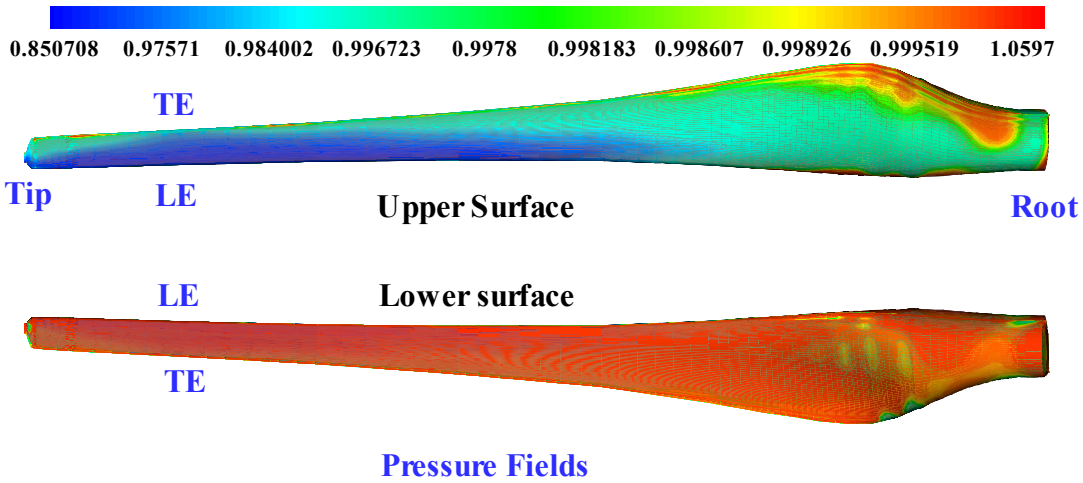

Figure 5. Pressure fields on the upper and lower surfaces of NAL's 500 kW wind turbine blade (deformed). Tilt = 7^o; Precone = 6^o; Tip speed ratio = 5.3; $M = 0.183$; $Re = 3.96$ million per meter.

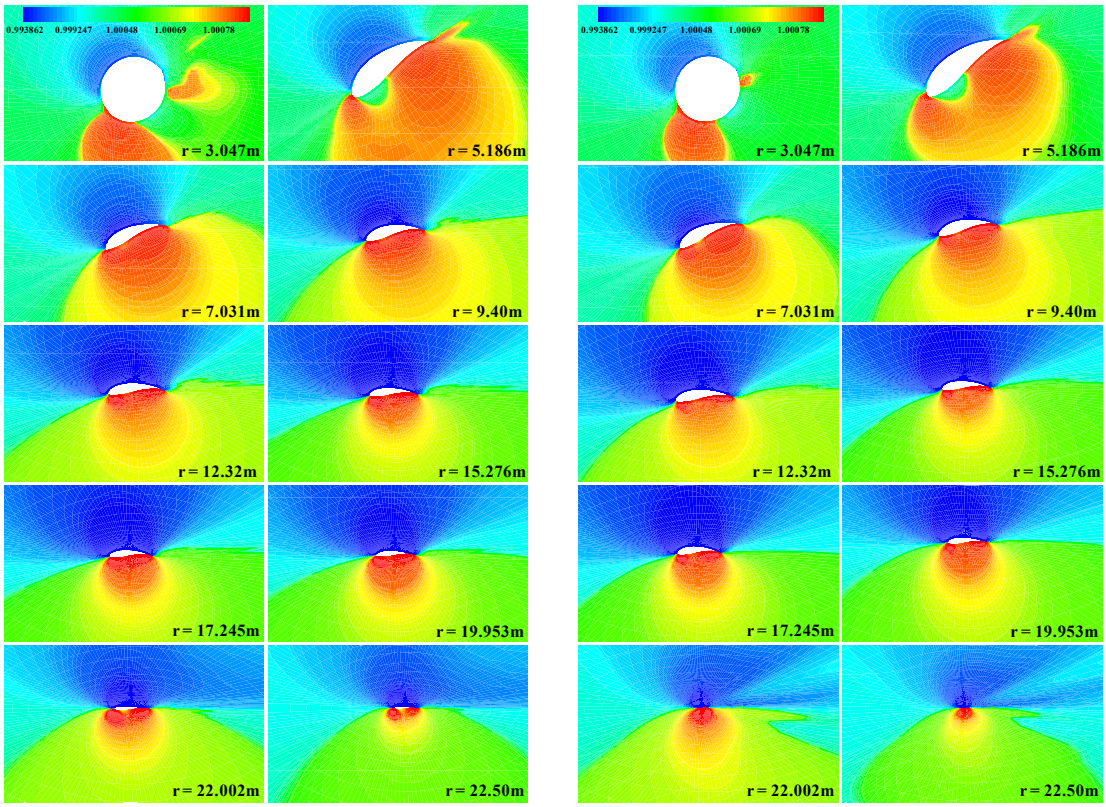

Figure 6. Pressure fields at different radial stations of the 500 kW straight (left) and deformed (right) wind turbine blades at wind speed of 12m/s. Tilt = 7^o; Precone = 6^o; Tip speed ratio = 5.3; $M = 0.183$; $Re = 3.96$ million per meter.

4 Concluding Remarks

Unsteady three-dimensional Reynolds averaged Navier-Stokes solver IMPRANS has been applied for computing flow over the straight and the deformed 500 kW wind turbine blades. The deformed blade generates around 8% more power against the straight blade at the rated wind speed of 12 meters per second. This increase in power for deformed blade is also seen in panel method calculations. It is, however, essential to confirm these results by actual field tests since the atmospheric boundary layer and turbulence and dust pollution are likely to have considerable effect on the aerodynamic power.

References

1. Baldwin, B. S. and Lomax, H., "Thin Layer Approximation and Algebraic Model for Separated Turbulent Flows", AIAA Paper No. 78-257, 1978.
2. Dutta, V., Dutta, P. K. and Sharanappa, "An Implicit RANS Solver for Unsteady Compressible Flow Computations", Proc. Seminar on State of the Art and Future Trends of CFD at NAL, NAL SP 0301, NAL, Bangalore, 2003 pp. 65-86.
3. Dutta P. K., Vimala Dutta, and Sharanappa, "Unsteady RANS Simulations Using Implicit Dual Time Stepping", Proc. Sixth Annual CFD Symposium, CFD Division of Aeronautical Society of India, Bangalore, August 11-13, 2003.
4. Dutta P. K., Vimala Dutta and Sharanappa, "RANS Computations of Flow Past Wind Turbine Blades", Proc. Seventh Asian Comp. Flu. Dyn. Conf. Bangalore, India, November 26-30, 2007.
5. Dutta, V., Sharanappa, and Dutta P. K., "Navier-Stokes Computations for a Helicopter Rotor Blade in Hover.", Proc. Eighth Annual CFD Symposium, CFD Division of Aeronautical Society of India, Bangalore, August 11-13, 2005, CP 18.

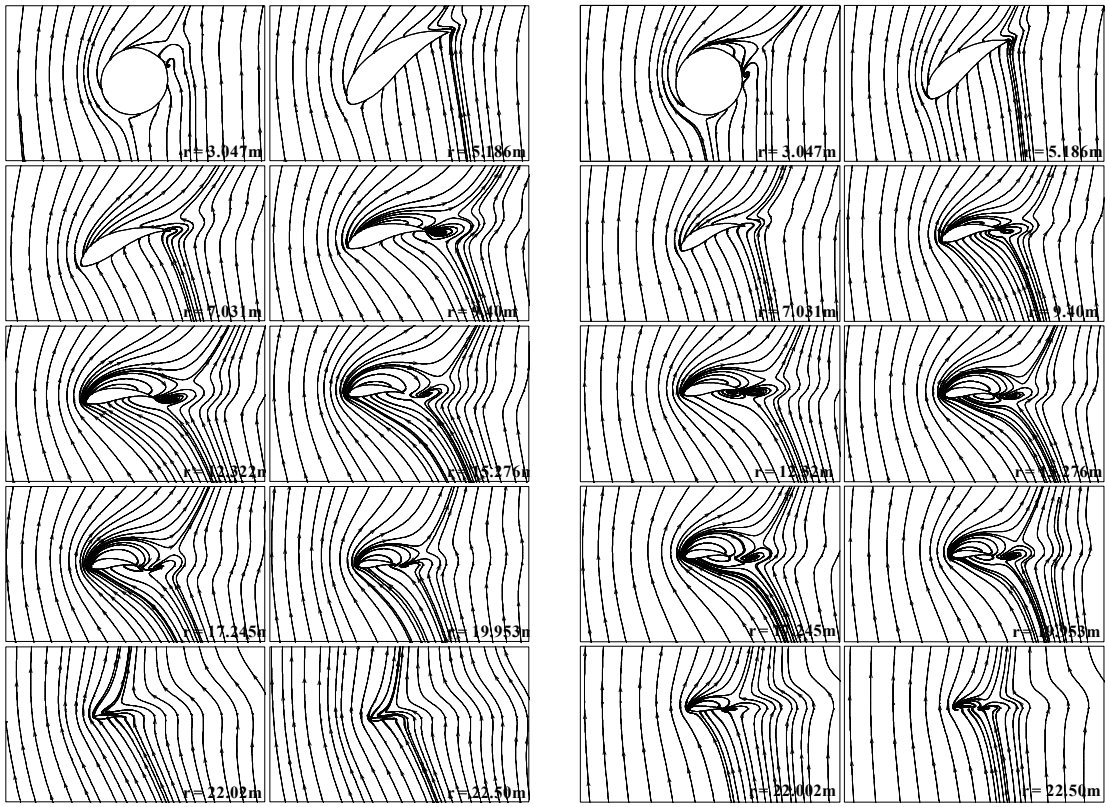

Figure 7. Streamtraces at different radial sections of the 500 kW straight (left) and bent (right) wind turbine blades at wind speed of 12m/s. Tilt = 7^o; Precone = 6^o; Tip speed ratio = 5.3; $M = 0.183$; $Re = 3.96$ million per meter

6. Beam, R. M. and Warming, R. E. (1978) An Implicit Factored Scheme for the Compressible Navier-Stokes Equations. AIAA J., 16, 393-402.
7. Gould, J. and Fiddes, S. P. (1992) Computational Methods for the Performance Prediction of HAWTs. J. Wind Eng. Ind. Aero., 39, 61-72.
8. Hernandez, J. and Crespo, A. (1987) Aerodynamics Calculation of the Performance of Horizontal Axis Wind Turbines and Comparison with Experimental Results. Wind Eng., 11, 4, 177-187.
9. Jones, C. (1983) Blade Element Performance in Horizontal-Axis Wind Turbine Rotors. Wind Eng., 7, 3, 129-137.
10. Premalatha and Mudkavi, V. Y. (2007) Aerofoil Design and Blade Stacking for a 500kW Horizontal-Axis Wind Turbine. PD CF 0702, National Aerospace Laboratories, Bangalore, India.
11. Rijs, R. and Smulders, P. (1990) Blade Element Theory for Performance Analysis of Slow Running Wind Turbines. Wind Eng., 14, 2, 62-79.
12. Sharanappa, Dutta, V. and Dutta, P. K. (2006) Viscous Unsteady Flow around a Helicopter Rotor Blade in Forward Flight. Proc. 9th Annual CFD Symposium, CFD Division of Aeronautical Society of India, Bangalore, August 11-12.
13. Srilatha, K. R. and Narayana, C. L. (2007) Aerodynamic Analysis of Aerofoils and Blades for a 500kW Horizontal-Axis Wind turbine. PD CF 0701, National Aerospace Laboratories, Bangalore, India.
14. Viterna, L. A. and Corrigan, R. D. (1981) Fixed Pitch Rotor Performance of Large Horizontal Axis Wind Turbines. NASA CP 2230.